Published online 1 February 2021

NAR Cancer, 2021, Vol. 3, No. 1 **1**
doi: 10.1093/narcan/zcab002

The DNA damage inducible lncRNA SCAT7 regulates genomic integrity and topoisomerase 1 turnover in lung adenocarcinoma

Luisa Statello [1,2], Mohamad M. Ali [1], Silke Reischl[1], Sagar Mahale[1], Subazini Thankaswamy Kosalai[1], Maite Huarte[2,3] and Chandrasekhar Kanduri [1,*]

[1]Department of Medical Biochemistry and Cell Biology, The Sahlgrenska Academy, Institute of Biomedicine, University of Gothenburg, SE-40530 Gothenburg, Sweden, [2]Department of Gene Therapy and Regulation of Gene Expression, Center for Applied Medical Research, University of Navarra, Pamplona 31008, Spain and [3]Institute of Health Research of Navarra (IdiSNA), 31008 Pamplona, Spain

Received November 16, 2020; Revised December 26, 2020; Editorial Decision January 04, 2021; Accepted January 06, 2021

ABSTRACT

Despite the rapid improvements in unveiling the importance of lncRNAs in all aspects of cancer biology, there is still a void in mechanistic understanding of their role in the DNA damage response. Here we explored the potential role of the oncogenic lncRNA SCAT7 (ELF3-AS1) in the maintenance of genome integrity. We show that SCAT7 is upregulated in response to DNA-damaging drugs like cisplatin and camptothecin, where SCAT7 expression is required to promote cell survival. SCAT7 silencing leads to decreased proliferation of cisplatin-resistant cells *in vitro* and *in vivo* through interfering with cell cycle checkpoints and DNA repair molecular pathways. SCAT7 regulates ATR signaling, promoting homologous recombination. Importantly, SCAT7 also takes part in proteasome-mediated topoisomerase I (TOP1) degradation, and its depletion causes an accumulation of TOP1–cc structures responsible for the high levels of intrinsic DNA damage. Thus, our data demonstrate that SCAT7 is an important constituent of the DNA damage response pathway and serves as a potential therapeutic target for hard-to-treat drug resistant cancers.

GRAPHICAL ABSTRACT

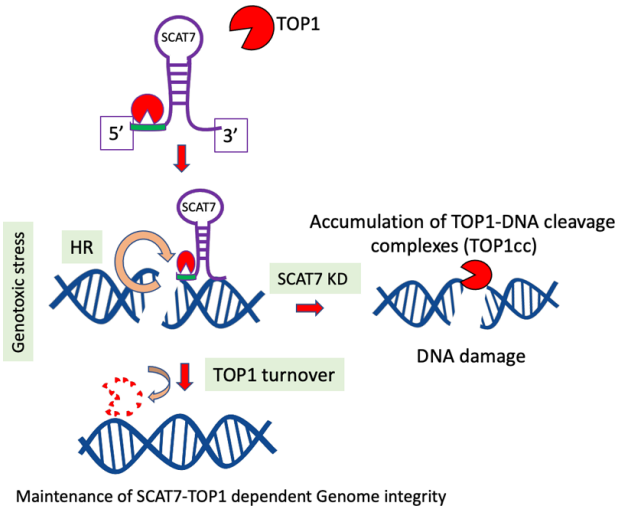

INTRODUCTION

Cells are constantly challenged by intrinsic as well as extrinsic stresses threatening genome stability (1). To maintain genomic integrity, eukaryotic cells have adapted a network of highly organized and coordinated cellular pathways, the so-called DNA damage response (DDR). DDR begins with the detection of DNA damage followed by activation of members of the phosphatidylinositol 3-kinase (PI3K)-like kinase (PIKK) family (2). The activation of DDR kinases triggers cascades of phosphorylation events and elicits diverse cellular responses, such as phosphorylation of histone H2A.X, activation of cell cycle checkpoints, recruitment of specific DDR pathway proteins leading to DNA repair or induction of apoptosis in cells that hyper accumulate unrepaired DNA (3,4).

*To whom correspondence should be addressed. Tel: +46 739600450; Email: kanduri.chandrasekhar@gu.se

The kinase ATR plays a critical role in orchestrating the response to replication stress ensuring replication fidelity, which is often compromised in cancer conditions. In the presence of destabilized and stalled replication forks, ataxia telangiectasia and Rad3 related (ATR) and its key transducers delay the progression through the S phase and stimulate homologous recombination (HR) (5). Moreover, ATR signaling is activated in the presence of topoisomerase (TOP1)-poison-dependent adducts, which is known to affect fork processivity (6) and take part in the maintenance of genome integrity in association with TOP1. Until recently, DNA damage has been mostly explored with a main focus on the phospho-signaling protein network responsible for the coordination of cell cycle arrest, activation of DNA repair and apoptosis. However, with the advent of high-throughput RNA-sequencing techniques, researchers have begun to explore the role of long non-coding RNAs (lncRNAs) in DDR (7–11). Despite our increased understanding of lncRNA role in DDR, more efforts are needed to fully elucidate the relationship between lncRNAs and DDR at the mechanistic level. Moreover, it is not clear how DNA damage occurs upon the loss of DNA damage-associated lncRNAs. At present, one of the main challenges in cancer treatment is the necessity to overcome the phenomenon of chemoresistance, which in turn requires the identification of new therapeutic approaches. In this context, DDR-associated lncRNAs are promising therapeutic targets due to their biology and their mode of action in finely regulating different cancer-associated molecular pathways.

In this study, we characterized the role of SCAT7 (also known as ELF3-AS1), an S phase-associated lncRNA harboring oncogenic properties, in the maintenance of genome integrity. We provide evidence that SCAT7 promotes HR through regulating ATR signaling during drug-induced DNA damage. Importantly, SCAT7 regulates the turnover of topoisomerase 1–DNA cleavage complexes (TOP1–cc) through maintaining the stability of TOP1 via an ubiquitin-dependent proteasome pathway. By analyzing phenotypic and molecular changes following SCAT7 depletion in cisplatin-resistant lung adenocarcinoma (LUAD/cDDP) cells in cell culture and xenograft models, we show that cisplatin and SCAT7 execute their effects on cancer cells through regulating common molecular pathways. Collectively, our results highlight the importance of SCAT7 in genome integrity and its potential as a therapeutic target for chemoresistant lung cancer.

MATERIALS AND METHODS

Cell lines and treatments

The human adherent lung adenocarcinoma cell lines A549 and H1975 were a kind gift of Bengt Hallberg's lab at the Department of Biochemistry and Cell Biology, University of Gothenburg. Cervical carcinoma HeLa cells (300194) and renal carcinoma Caki-2 cells (300140) were purchased from CLS cell lines service, Germany. The bronchioalveolar carcinoma H358 (ATCC No. CRL-5807), and the bronchial epithelium BEAS-2B cells (ATCC No. CRL-9609) were purchased from ATCC. MDA-MB-468 (ACC378) cells were purchased from DSMZ, Germany. A549 and HeLa cells were cultured in Dulbecco's modified Eagle's medium (DMEM) (Gibco, Life Technologies, USA); HN-HeLa (HeLa NHEJ Reporter Cell Line) cells, purchased from TopoGen (Buena Vista, CO, USA), were cultured in DMEM medium supplemented with 200 μg/ml G418. H1975, H358 and Caki-2 cells were cultured in RPMI-1640 medium (Gibco, Life Technologies, USA). All medium were supplemented with 10% fetal bovine serum (Gibco, Life Technologies, USA), 1% penicillin-streptomycin (Gibco, Life Technologies, USA). BEAS-2B cells were cultured in BEGM Bronchial Epithelial Cell Growth Medium with supplements provided in the BEGM™ BulletKit™ (Lonza; Walkersville, MD, USA). All cells were grown in cell culture incubator at 37°C and 5% CO_2. All cells were tested negative for Mycoplasma. For viability assay and quantitative polymerase chain reaction (qPCR), A549 and H358 cells were treated with 15–20 μM cisplatin (Merck KGaA, Darmstadt, Germany) for 24–48 h. For drug treatments of A549 cells, camptothecin (CPT) was used at 15 μM, nutlin-3a and etoposide at 20 μM and doxorubicin (Sigma Aldrich, Germany) was used at 5 μM, at the time points indicated. For both western blot analysis following DNA damage and DNA damage induction in HR assay, A549 cells were treated with 15 μM cisplatin for 24–48 h. For TOP1 turnover experiments, A549 CTRL and *SCAT7* KD A549 cells were treated with 15 μM CPT (Merck KGaA, Darmstadt, Germany) for 2 h; for combined treatment 15 μM CPT was added for 2 h after overnight pre-treatment with 15 μM of the proteasome inhibitor MG132 (Calbiochem, Merk). For TOP1 IP experiments, A549 cells were pre-treated with 14 μM MG132 overnight followed by treatment with 15 μM CPT for 2 h. For TOP1-ICE (*In vivo* Complex of Enzyme) assay, cells were treated with 50 μM CPT for 1 h.

Cell fractionation

1×10^7 cells were collected by trypsinization. Cell pellet was resuspended in 200 μl of cytoplasmic lysis buffer (10 mM Tris–HCl [pH 7.5], 150 mM NaCl, 0.15% NP-40 supplemented with 1 × complete protease inhibitor cocktail (Roche) and 10 U/ml SUPERaseIN (ThermoFisher Scientific), incubated on ice for 5 min and layered the lysate on 500 μl of sucrose buffer and centrifuged at 12 000 × *g* for 10 min. Trizol was added to the supernatant with cytoplasmic fraction to isolate cytoplasmic RNA. The remaining pellet was washed once with nuclei wash buffer (1 mM ethylenediaminetetraacetic acid (EDTA), 0.1% Triton X-100 supplemented with 1 × complete protease inhibitor cocktail and 20 U/ml SUPERaseIN. Subsequently, nuclear pellet was resuspended in 200 μl of glycerol buffer (20 mM Tris–HCl [pH 7.5], 75 mM NaCl, 0.5 mM EDTA, 50% glycerol, 0.8 mM DTT, 1 × complete protease inhibitor cocktail and 20 U/ml SUPERaseIN) and 200 μl of nuclei lysis buffer (20 mM HEPES (pH 7.5), 300 mM NaCl, 1M urea, 0.2 mM EDTA, 1 mM DTT, 1 × complete protease inhibitor cocktail and 20 U/ml SUPERaseIN). After centrifugation, supernatant containing the soluble nuclear fraction and chromatin pellet were separately lysed with TriZol and processed for RNA isolation.

Generation of cisplatin-resistant A549 cells

We have generated cisplatin-resistant A549 cells (A549/cDDP) from the parental A549 cell line over the course of 8 months. The cells were cultured initially at the IC_{50} for 72 h, followed by 72 h with normal medium to isolate a few surviving clones. Following this, we cultured the obtained cell population at $IC_{12.5}$ constantly. After few weeks, we increased the concentration to IC_{25}, and finally after 8 months we were able to grow the cells in the IC_{50} for the parental cell line.

Transient and stable transfections

LNA GapmeRs targeting SCAT7 along with negative control were obtained from QIAGEN. About 20–30 nM of *SCAT7* targeting GapmeRs were transfected into A549, H1975, H358, BEAS-2B, MDA-MB-468, Caki-2 and HN-HeLacells using Lipofectamine RNAiMAX (Invitrogen, CA, USA) following the manufacturer's instructions. Stable A549 cells were generated using Lentifect™ Purified shRNA lentivirus particles targeting SCAT7 or negative control designed and synthesized by GeneCopoeia™, referred as SCAT7_sh1 and SCAT7_sh2. Transduction efficiency was established through GFP visualization. We also generated stable SCAT7 KD cell lines with custom MISSION Lentiviral pLKO.1 transduction particles obtained from Sigma-Aldrich, referred as SCAT7_sh3 and SCAT7_sh4. All stable KD cells were selected using 3 μg/ml puromycin and KD efficiency was evaluated by RT-qPCR. For TOP1 half-life studies, A549 cells were stably transduced with lentiviral particles containing either pLVX-Tet-One (empty vector control) or pLVX-Tet-One *SCAT7* (788 nt). Cells were seeded and were treated with CPT (14 μM) and cycloheximide (20 μM) and harvested after 60 and 120 min. SCAT7 RNA was overexpressed 12-fold compared to empty vector control. After discovering that the *SCAT7* sequence was curated on ENSEMBL (NR_146472.1, 831 nt), we cloned this curated sequence from A549 cDNA into pLVX-Tet-One via EcoRI and AgeI restriction sites. Different *SCAT7* fragments (1. 1–210, 2. 1–420, 3. 1–639, 4. 211–630) were also cloned accordingly. All sequences were verified by sequencing. Lentiviral particles were generated with the vectors containing different *SCAT7* fragments and transduced them into A549 cells. The transduced cells were selected with the addition of puromycin (3 μg/ml). Overexpression efficiency was evaluated by RT-qPCR. The sequences of siRNAs, shRNAs, LNAs and primers are listed in Supplementary Table S1.

RNA, DNA isolation and qPCR

Total RNA from all cell treatments was isolated using ReliaPrep RNA cell miniprep system (Promega) according to the manufacturer's protocol. For RNA isolation from mouse tumors, we first disrupted the tumors using Stainless steel beads, 5 mm (QIAGEN GmbH, Hilden) in a tissue homogenizer; then RNA isolation was performed as previously described. DNA isolation from HR assay samples was performed using the Wizard Genomic DNA purification kit (Promega).

RNA sequencing, differential expression, pathway analysis and network analysis

RNA samples from A549 parental cells, A549/cDDP and SCAT7 KD A549/cDDP cells were sequenced using the HISeq 4000 Illumina system by Novogene. RNA-seq analysis was performed following the common Novogene pipeline: reads were aligned to the genome assembly GRCh38 and processing was performed using annotation from Ensembl release 82. Alignment was performed using Tophat2, gene expression levels were quantified using HT-Seq. Gene expression analysis was performed using DE-Seq, genes were considered differentially expressed, if they were upregulated or downregulated with minimum $\log_2$ fold change ± 1 in the two biological replicates with and FDR $\leq$ 0.05. Gene Ontology (GO) and pathways analysis of differentially expressed protein-coding genes were performed using GeneSCF ($P \leq 0.05$) and considered only if bearing at least 10 differentially genes expressed in the pathway (12).

The list of SCAT7 binding proteins identified by ChOP (13) was submitted to Cytoscape (version 3.6.0) using the tool Reactome FiViz to retrieve the network of first protein interactors (14). Pathway analysis on the SCAT7 binding proteins and the interacting network was performed using the Reactome FI plugin for Cytoscape. Pathways were considered significant at FDR < 0.05 and number of genes in the pathway ≥ 20.

Western blot and immunofluorescence

Protein extracts were prepared by using RIPA buffer (150 mM NaCl, 50 mM Tris pH8, 1% Triton X-100, 0.5% NA DOC, 0.1% sodium dodecyl sulfate (SDS)) with 1× proteases and phosphatases inhibitors (Pierce-Thermo Scientific, Rockford, USA), and quantified by BCA assay (Pierce-Thermo Scientific, Rockford, USA). About 40–50 μg proteins were loaded in a 4–12% (w/v) Bis-Tris SDS-polyacrylamide gel electrophoresis (SDS-PAGE) (Invitrogen) together with SeeBlue Plus2 Prestained Standard (Invitrogen) or PageRuler Plus Prestained Protein ladder (Thermo Scientific) and transferred into a nitrocellulose membrane (Amersham, Germany). After Ponceau staining blots were immunostained with primary antibodies overnight at 4°C with gentle shaking. List of all primary antibodies used and relative concentrations are listed in Supplementary Table S1. All primary antibodies were diluted in PBST with 5% BSA (Sigma-Aldrich). Horseradish peroxidase-conjugated secondary antibodies anti-mouse and anti-rabbit antibodies were diluted at 1:5000 in PBST with 1% BSA. Blots were detected using SuperSignal West Pico Chemiluminescent Substrate (Pierce-Thermo Scientific) and imaged in a Bio-Rad ChemiDoc imaging system. Densitometry analysis was performed using Image Studio Lite. Experiments were performed at least in biological triplicates. For immunofluorescence (IF), cells were seeded on coverslips in 24- or 6-well plates, fixed in 1% formaldehyde in phosphate-buffered saline (PBS) for 15 min at RT and permeabilized with 0.25% Triton X-100 for 20 min at RT. Cells were blocked with 1% BSA in PBST for 30 min and then incubated with primary antibodies diluted in PBST with 1% BSA for 1 h at RT or overnight at 4°C with gentle shaking followed by appropriate Alexa Fluor™ 555 or

488 goat anti-mouse or anti-rabbit secondary antibodies (Invitrogen) at 1:500 dilution in PBST BSA 1%. Coverslips were mounted with DAPI-containing Vectashield mounting medium (Vector Laboratories, Burlingame, CA, USA). Images were acquired using EVOS™ FL Auto Imaging System (Life Technologies) and/or confocal microscope (Carl Zeiss).

DNA combing assay

For DNA fiber assay, A549 cells were transiently transfected with SCAT7 targeting GapmeR along with negative control as previously described. Forty-eight hours post transfection, cells were subjected to two consecutives 30 min pulses with 0.1 mM 5-Chloro-2'-Deoxyuridine (CldU) and 0.1 mM 5-Iodo-2'-Deoxyuridine (IdU) (Sigma Aldrich) followed by three cold PBS washes. Cells were harvested and counted. 50×10^5 cells/sample were used for gel plugs preparation using the FiberPrep DNA extraction kit (Genomic Vision, Begneux, France) and Gel plug molds (Bio-Rad, Hercules, CA, USA) following the manufacturer's protocol. DNA samples in agarose plugs were sent to Genomic Vision facility (Bagneux, France) for DNA stretching into coverslips and data acquisition on the FiberVision platform (Genomic Vision). We performed DNA fiber analysis using the software FiberStudio version 0.9.12 (Genomic Vision).

Non-homologous recombination

For non-homologous end joining (NHEJ) recombination experiments, transiently transfected HN-HeLa cells with SCAT7 targeting GapmeR, were seeded in 96-well plates. Twenty-four hours post-transfection, doxycycline (dox) was added to the medium to induce I-Sce1 gene and activate NHEJ for up to 5 days. To evaluate NHEJ, images were acquired using EVOS™ FL Auto Imaging System (Life Technologies), and GFP positive cells were counted using Fiji software.

Homologous recombination

For HR analysis we used the HR kit from Norgen Biotek Corporation (Canada), providing two different plasmids (dl-1 and dl-2) each containing a defective lacZ cassette that through an event of HR form a functional lacZ cassette. Briefly, 40×10^4 A549 cells/well in 24-well plates were first transfected with *SCAT7* targeting LNA GapmeRs following the protocol described earlier. Twenty-four hours post transfection, cells were transfected with 500 ng dl-1 plasmid and dl-2 plasmids together for HR assay, dl-1 and dl-2 alone for negative control, and a positive control plasmid, using GeneJet reagent (SignaGen Laboratories). Twenty-four hours after plasmid transfection, we induced DNA damage with 5 μM cisplatin for 24 h, and treated control cells with dimethyl sulfoxide (DMSO) only. Cells were harvested and DNA was isolated with QIAmp DNA Mini Kit (QIAGEN). The rate of HR was evaluated by RT-qPCR using the Assay Primer Mixture (detecting the recombined LacZ sequence) and Universal Primer Mixture (detecting the plasmid backbone) supplied in the kit. For RT-qPCR we used the following conditions: initial denaturation at 95°C for 3 min, then 95°C for 15 s, 61°C for 30 s and 72°C for 1 min repeated for 40 cycles.

In vivo complex of enzyme assay

TOP1–cc were identified using the *In vivo* Complex of Enzyme (ICE) assay kit from TopoGEN (Buena Vista, CO, USA). Briefly, 3.5×10^4 A549 cells were transfected with SCAT7 LNA GapmeR for 48 h in 35 mm dishes before treatment with 50 μM CPT or DMSO for 1 h. Stable *SCAT7* KD A549 cells were seeded at 3.5×10^4 24 h before the treatments with 50 μM CPT or DMSO. Cells were lysed in lysis buffer A provided in the kit and ethanol was added to precipitate the DNA. Clumped DNA was retrieved and washed three times with room temperature 75% ethanol followed by 2 min centrifugation at 21 000 × *g* and DNA solubilization with brief sonication for 1 s to shear high MW genomic DNA. DNA was quantified by Nano-Drop. Covalent complexes were transferred into a nitrocellulose membrane using a Bio-Dot SF (slot format) (Bio-Rad). Membrane was blocked with PBST containing 5% BSA for 30 min and TOP1–cc complexes were detected using a moAb anti-TOP1–cc overnight followed by 1 h incubation with HRP-conjugated anti-mouse secondary antibody (1:5000 in PBST in 1% BSA). Densitometry analysis was performed using Image Studio Lite. Experiments were performed in duplicates.

RNA immunoprecipitation

For SCAT7-TOP1 interaction validation, A549 cells (20×10^6) were harvested and crosslinked using 1% formaldehyde for 10 min with gentle rotation. Fixation was quenched with 125 mM glycine for 5 min at RT. Cells were pelleted by centrifugation at 1200 rpm at 4°C for 10 min and resuspended in 1× nuclei isolation buffer (1.28 M sucrose; 40 mM Tris–HCl pH 7.5; 20 mM MgCl2; 4% Triton X-100; 100 U/ml RNAse inhibitors, 1× protease inhibitor), incubated on ice for 20 min, mixing the solution every 5 min. Lysate was then centrifuged at 2500 rpm for 7 min at 4°C, and after removal of the suspension containing cytoplasmic fragments, nuclear pellet was resuspended in RIPA lysis buffer (150 mM NaCl, 50 mM Tris, 0.5% sodium deoxycholate, 0.2% SDS, 1% NP-40) supplemented with protease and RNase inhibitors. Lysates were sonicated in a Diagenode sonicator for five cycles (30 s ON and 30 s OFF) or more until the lysate became clear followed by centrifugation at 11 000 rpm for 10 min at 4°C. Lysates were incubated overnight with TOP1 antibody at 4 μg/mg lysate (Bethyl Laboratories) or rabbit IgG at 4°C with constant rotation, after removal of 1% lysate to serve as input. The immune complexes were allowed to bind to G/A Dynabeads (ThermoFisher Scientific) for 3.5 h at 4°C with gentle rotation, followed by two washes in RIPA low salt buffer (0.1% SDS, 1% Triton-X 100, 2 mM EDTA, 20 mM Tris–HCl, 15 mM NaCl, 0 mM PMSF and 50 units/ml RNasin) and two washes in RIPA high salt buffer (0.1% SDS, 1% Triton-X 100, 2 mM EDTA, 20 mM Tris–HCl, 500 mM NaCl, 0.5 mM PMSF and 50 units/ml RNasin). Immune complexes were eluted in Proteinase K buffer supplemented with RNAsin, and de-cross linking was carried out for 45 min at 55°C with moderate vibration. Immune complexes were separated from the beads

and RNA was isolated with TriZol (ThermoFisher Scientific). Isolated RNA was used for cDNA synthesis followed by qPCR along with the RNA isolated from input samples. The sequence of primers used is listed in Supplementary Table S1.

Chromatin oligo-affinity precipitation (ChOP)

20×10^6 cells were collected for each precipitation and cross-linked with 10 ml of 1% formaldehyde in PBS for 10 min at RT with gentle rotation. The reaction was quenched with 125 mM glycine for 5 min with gentle rotation at RT. The fixed cells were washed twice with ice-cold PBS and spun down for 5 min at 2000 × *g* in the cold. The cell pellet with 2 ml of buffer A (3 mM MgCl2, 10 mM Tris–HCl; pH 7.4, 10 mM NaCl, 0.5% v/v NP-40, 0.5 mM PMSF and 100 units/ml RNase inhibitor) on ice for 20 min, with gentle pipetting every 5 min. The nuclei were harvested by centrifugation at 14 000 × *g* for 15 min at 4°C. The supernatant was discarded and the pelleted nuclei were re-suspended in 1.2 ml of buffer B (50 mM Tris–HCl; pH 7.4,10 mM EDTA, 0.5% Triton X-100, 0.1% SDS, 0.5 mM PMSF and 100 units/ml RNase inhibitor). We lysed the nuclei on ice for 40 min with thorough pipetting every 5 min. Following this, we added another 1.2 ml of buffer C (15 mM Tris–HCl; pH 7.4, 150 mM NaCl, 1 mM EDTA, 1% Triton X-100, 0.5 mM PMSF and 100 units/ml RNase inhibitor) and incubated the nuclei for 15 min on ice. Lysates were sheared using a Bioruptor sonicator (Diagenode) for 20 cycles at a high pulse. We used a pool of biotinylated probes (10 μM) targeting *SCAT7* (positive probes) to pull down the lncRNA as described before (13). We used LacZ biotinylated probes as a negative control and control which is complementary to the positive probes. Sonicated lysates were incubated overnight on gentle rotation at 4°C with each individual set of mixed probes. The lysate/probes mixtures were incubated for 3 h at 4°C on rotation with streptavidin-coupled Dynabeads (ThermoFisher Scientific). Beads were then washed twice for 5 min each at 4°C with low salt buffer (20 mM Tris–HCl, pH 7.9, 150 mM NaCl, 2 mM EDTA, 0.1% SDS, 1% TritonX-100, 0.5 mM PMSF and 50 units/ml RNase inhibitor). Two more washes with high salt buffer (20 mM Tris–HCl, pH7.9, 500 mM NaCl, 2 mM EDTA, 0.1% SDS, 1% Triton X-100, 0.5 mM PMSF and 50 units/ml RNase inhibitor) were applied for 5 min each at 4°C. Finally, the beads-bound proteins were washed twice with PBS at RT. Different species of RNA–protein complexes were further eluted by heating and vigorous mixing of the beads at 80°C for 15 min with 50 μl of 1× Tris-Glycine SDS sample buffer. The protein of interest was detected using immunoblotting as described in the previous section.

Protein immunoprecipitation (IP) of ubiquitinated TOP1

For immunoprecipitation experiments, 3×10^6 SCAT7 KD cells and control cells were treated with CPT or DMSO control for 2 h in the presence of 15 μM MG132. Cells were then collected and lysed in ice cold lysis buffer (150 mM NaCl, 50 mM Tris, 2.5 mM EDTA, 1% NP-40, 0.1% SDS, 10 mM NEM, 1 × protease inhibitors, 15 μM MG132). Cells were lysed by incubation at 4°C for 10 min followed by a brief sonication. About 1% of the lysate was stored as input and eluted in SDS elution buffer for western blot. Control IgG or TOP1 antibody (Bethyl Laboratories) were incubated overnight with the lysate. 50 μl of G/A magnetic Dynabeads (ThermoFisher Scientific) were washed three times with lysis buffer at 4°C and incubated with the antibody/lysate mixture for 2 h at 4°C with gentle rotation. Immune precipitates were washed twice in lysis buffer at 4°C for 5 min each, followed by two washes with lysis buffer supplemented with 800 mM NaCl. Washed beads were re-suspended in 1× Tris-Glycine SDS sample buffer (ThermoFisher Scientific) and boiled for 5 min. Eluted immune precipitates were detected by SDS-PAGE followed by immune detection using FK2 antibody.

Mouse xenografts

Animal studies were performed in accordance to our Ethical permit (No: 5.8.18–02708/2017), reviewed and approved by the Animal Ethical Review Board, University of Gothenburg, Sweden.

For xenograft experiments, 2.5×10^6 A549 parental cells or A549/cDDP cells in PBS with 20% Matrigel (Corning) were injected in the right flank of 5–6 weeks old Balb/C nude mice (Janvier labs). When tumors became measurables, we divided the mice in different groups for treatment. A549 xenografts were divided in four groups ($n = 4$) as follows: non-treated, cisplatin (5 mg/Kg), SCAT7 GapmeR (100 pmoles/mouse) + cisplatin (5 mg/Kg), control GapmeR (100 pmoles/mouse) + cisplatin (5 mg/Kg). A549/cDDP xenografts were divided in six groups ($n = 4$) as follows: non-treated, cisplatin (5 mg/Kg), SCAT7 GapmeR (100 pmoles/mouse), SCAT7 GapmeR (100 pmoles/mouse) + cisplatin (5 mg/Kg), control GapmeR (100 pmoles/mouse), control GapmeR (100 pmoles/mouse) + cisplatin (5 mg/Kg). The therapeutic regimen was performed as peritumoral subcutaneous injections of the previously described combinations diluted in PBS with the following schedule: day 1 GapmeR injections and day 2 cisplatin injection for at least five cycles, measuring tumor size every 2 days. Mice were weighted and checked daily for any sign of stress or sickness. Experiments were terminated when tumors grew over 1 cm^3, or when mice were showing signs of discomfort or 10% gain or loss of weight. Tumor sizes were evaluated using the following formula: (length [L] × width [W] × height [H])/2. Tumor growth was calculated starting from the first day of treatment, calculating ΔV at every time point, relative to the starting volume.

RESULTS

SCAT7 prevents accumulation of DNA damage

Recently, we characterized the oncogenic role of the *SCAT7/ELF3-AS1* gene, located on chromosome 1 and encoding an S-phase enriched antisense lncRNA (Figure 1A), in regulating FGF/FGFR signaling in lung and renal cancer cells (13). Given that lncRNA-protein interaction dictates their modes of actions, we investigated *SCAT7*-interacting proteins for relevant S-phase functions.

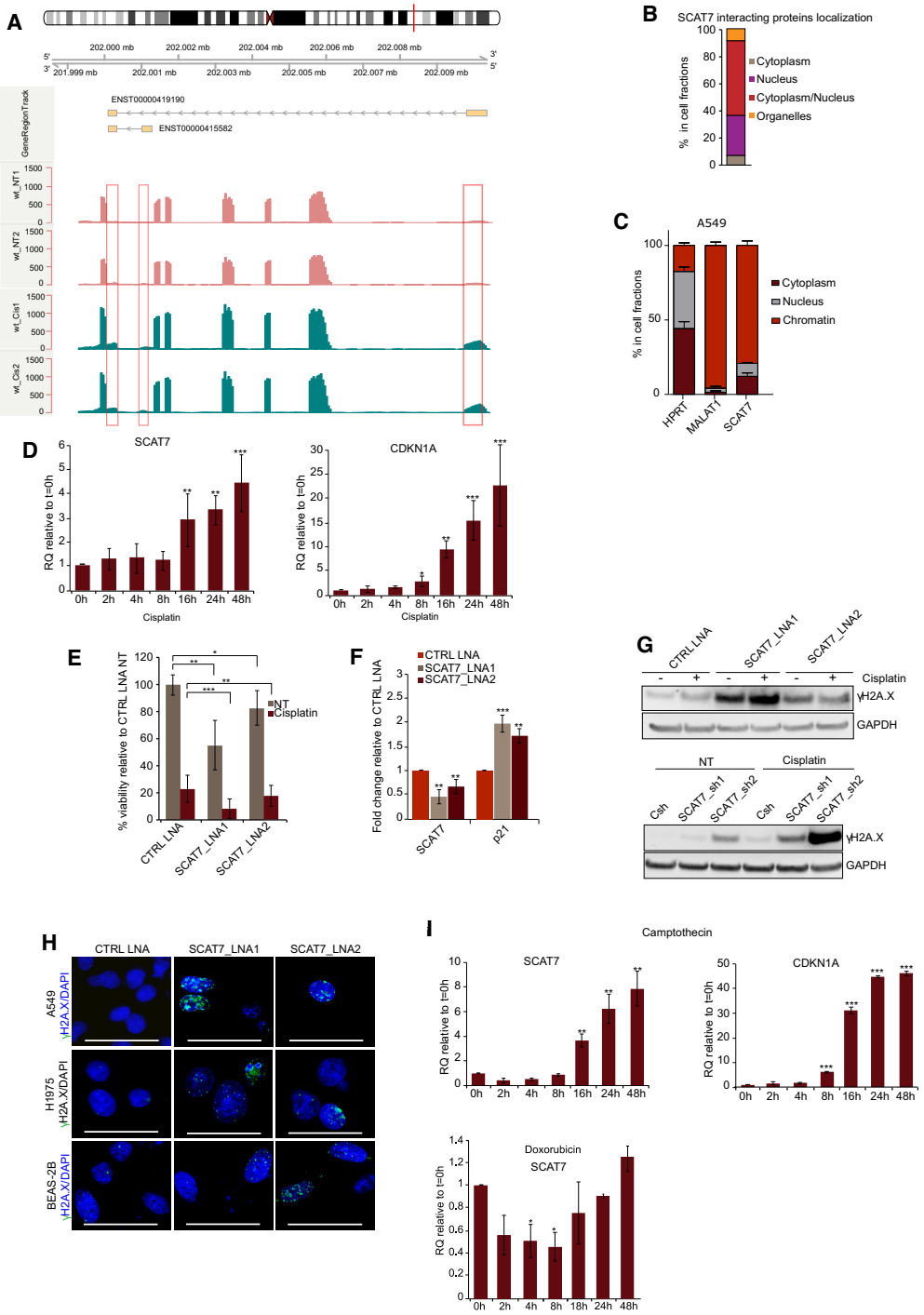

Figure 1. SCAT7 regulates genome integrity and DNA repair. (**A**) Physical map showing *SCAT7* (ELF3-AS1) locus, and underneath the maps showing the RNA-seq tracks for non-treated and cisplatin treated (24 h) WT A549 cells in two biological replicates (wt_NT1–2, wt_Cis1–2). Track height represents normalized read depth. (**B**) Schematic of sub-cellular localization of SCAT7 protein interactors. (**C**) Subcellular localization of SCAT7 lncRNA and control lncRNAs HPRT and MALAT1, determined by cytoplasm-nuclear-chromatin fractionation and RT-qPCR in A549 cell line. Graph shows mean ± SD of two independent experiments. (**D**) RT-qPCR analysis of cisplatin-treated A549 cells in a time course of 48 h shows that *SCAT7* is induced along with *CDKN1A*, the main marker of cisplatin response. (**E**) MTT assay on *SCAT7* KD A549 cells with LNAs before and after treatment with cisplatin (24 h). NT = non-treated. Data are represented as percentage compared to untreated cells transfected with negative control. Mean values of at least three independent experiments are shown and statistical significance was derived using a two-tailed unpaired Student's *t*-test. Data are plotted as mean ± SD (*$P \leq 0.05$; **$P = 0.01$ 0.001; ***$P < 0.001$). (**F**) qPCR showing the expression of *CDKN1A* in *SCAT7*-depleted cells. (**G**) Western blot showing DNA damage marker γH2A.X in A549 cells transfected with LNA GapmeRs or transduced with shRNA particles. Representative experiments of at least three biological replicates; (**H**) IF images showing γH2A.X levels in the indicated cell lines following *SCAT7* KD using LNA-GapmeRs. Scale bar 50 μm. (**I**) *SCAT7* expression following treatment with the topoisomerase I and topoisomerase II inhibitors CPT (15 μM) and doxorubicin (5 μM), respectively, in a time course of 48 h. For (D), (F) and (I) experiments were performed in biological triplicates and data are plotted as mean ± SD (*$P \leq 0.05$; **$P = 0.01$ 0.001; ***$P < 0.001$). Significance was derived using two-tailed unpaired Student's *t*-test.

To this end, we scrutinized the list of previously identified SCAT7 interactors, which includes several proteins with key roles in chromatin remodeling (BRD9) (15), DNA unwinding, replication and repair (XRCC5, TOP1, SFPQ) (16–18), sister chromatid cohesion and segregation (SMC3, NKAP) (19,20) and ubiquitination (RBBP6, RBBP7, USP16) (21–23). We determined the subcellular localization of SCAT7–protein interactors using the subcellular localization database compartments (https://compartments.jensenlab.org), where 30% of the interacting proteins exhibited nuclear localization, whereas only 6% of the proteins harbor exclusive cytoplasmic localization. The remaining proteins are distributed between the cytoplasmic and nuclear compartments (Figure 1B). These data are in concordance with SCAT7 sub-cellular distribution and its functions in the nuclear and chromatin fractions in several cancer cell lines (13) (Figure 1C and Supplementary Figure S1A).

To get a broader understanding of the biological relevance of the SCAT7 interactome, we performed a protein network analysis of SCAT7 nuclear interactors using the plugin BinGO (24). The analysis identified five functional groups: DNA repair, infectious disease, transport of mature RNAs to the cytoplasm, FGFR signaling and epigenetic regulation of gene expression (Supplementary Figure S1B and Table S2). This functional pattern, together with our previous knowledge on SCAT7 role in pro-proliferative and anti-apoptotic functions, opened an intriguing possibility for the role of SCAT7 in genome integrity maintenance, especially in the light of recent findings connecting lncRNAs to genome integrity through similar pathways and protein interactors (25). Therefore, we decided to further explore the contribution of SCAT7 to the DNA damage phenotype. When we challenged the LUAD cell line A549 with the DNA damaging agent cisplatin, *SCAT7* was activated (Figure 1A). To test if the *SCAT7* gene activation was an early or late event in cisplatin challenged cells, we performed a time course of cisplatin treatment over 48 h. Interestingly, *SCAT7* and *CDKN1A*, which encodes the p21 protein, were activated as late transcriptionally events. They showed similar expression patterns except that *SCAT7* started showing activation 16 h post cisplatin treatment, whereas the increase of *CDKN1A* expression was detected at 8 h. We have observed their gradual increase in expression post treatment up to 48 h (Figure 1D). Based on *SCAT7* expression dynamics in response to cisplatin treatment, we hypothesize that *SCAT7* activation represents a pro-survival response to cisplatin-induced DNA damage, antagonizing cisplatin-dependent cell cycle arrest and apoptosis which are shown to be mediated by *CDKN1A* (26). Concordant with this, SCAT7 knockdown (KD) further reduces cell viability upon cisplatin treatment (Figure 1E and Supplementary Figure S1C). Furthermore, SCAT7 KD cisplatin-treated cells exhibited higher levels of cleaved PARP, an indicator of caspase 3 activity, and lower levels of apoptotic inhibitor XIAP (Supplementary Figure S1D), suggesting that the combined treatment enhances apoptotic response compared to cisplatin treatment alone. At the transcriptional level, *CDKN1A* was activated in SCAT7 depleted cells (Figure 1F and Supplementary Figure S1E). KD of *SCAT7* in normal and cancer cell lines induces γH2A.X levels, the main marker of double strand breaks (DSBs) (Figure 1G and H; Supplementary Figure S1F). The transcriptional activation of *CDKN1A* following SCAT7 KD is concordant with the G1/S arrest, and increased DNA damage. Despite the similar expression trend of *SCAT7* and *CDKN1A*, p53 is dispensable for *SCAT7* activation. For example, in $p53^{-/-}$ LUAD H358 cells, in response to cisplatin treatment, expression of canonical p53 responsive protein-coding genes and the lncRNA *NEAT1* was greatly reduced or abolished, whereas *SCAT7* expression was activated, further reinforcing p53 independent transcriptional regulation of *SCAT7* (Supplementary Figure S1G).

Next, we tested the hypothesis that *SCAT7* activation mediates tolerance in response to various cellular stress factors. To this end, we treated A549 cells with non-genotoxic as well as genotoxic drugs inducing replication stress and DNA damage through different mechanisms. For example, cells treated with topoisomerase II (TOP2) poisons etoposide and doxorubicin, or MDM2 inhibitor nutlin-3a showed only a minor, if any, *SCAT7* activation (Figure 1I; Supplementary Figure S1H and I). On the other hand, challenging A549 with heat shock (45°C for 90 min) followed by 2 h recovery decreased the *SCAT7* expression (Supplementary Figure S1J). However, when we challenged A549 cells with CPT, a specific TOP1 inhibitor, we observed a similar activation pattern of *SCAT7*, as seen in cisplatin but with much higher induction (Figure 1I). TOP1 and TOP2 inhibitors activate distinct repair pathways, and in particular, HR is primarily involved in repairing single-ended DSBs induced by TOP1 inhibitors (27,28). Therefore, we hypothesize that SCAT7 might be a regulator of DDR, acting through parallel pathways involved in response to cisplatin and CPT treatments. Moreover, the spontaneous DSBs observed in *SCAT7*-depleted cells suggest that SCAT7 contributes to the maintenance of genomic stability.

SCAT7 regulates S-phase checkpoint and mediates HR and replication stress

In an attempt to understand functional connection between SCAT7 and DNA damage, we addressed its role in the activation of the genomic surveillance pathway in over-replicating cancer cells, or in response to treatment with genotoxic agents interfering with replication. The first mediator of such pathways is the kinase ATR, which is promptly activated when DNA replication is endangered by DNA damage. Besides blocking S-phase progression through the phosphorylation of its downstream effector CHK1, ATR has been tightly associated with the activation of DNA repair pathways, and its impairment or inhibition interferes with HR (29–31).

Based on this, we first evaluated the activation of ATR pathway in SCAT7 KD cells in the presence of drug-induced DNA damage. Interestingly, ATR signaling is compromised in SCAT7 KD cells, as shown by the decrease of ATR and CHK1 phosphorylation in western blot and IF (Figure 2A–D and Supplementary Figure S2A), suggesting that SCAT7 is involved in the regulation of ATR activation. The impairment of ATR signaling upon SCAT7 KD is due to post-transcriptional events, as we did not observe

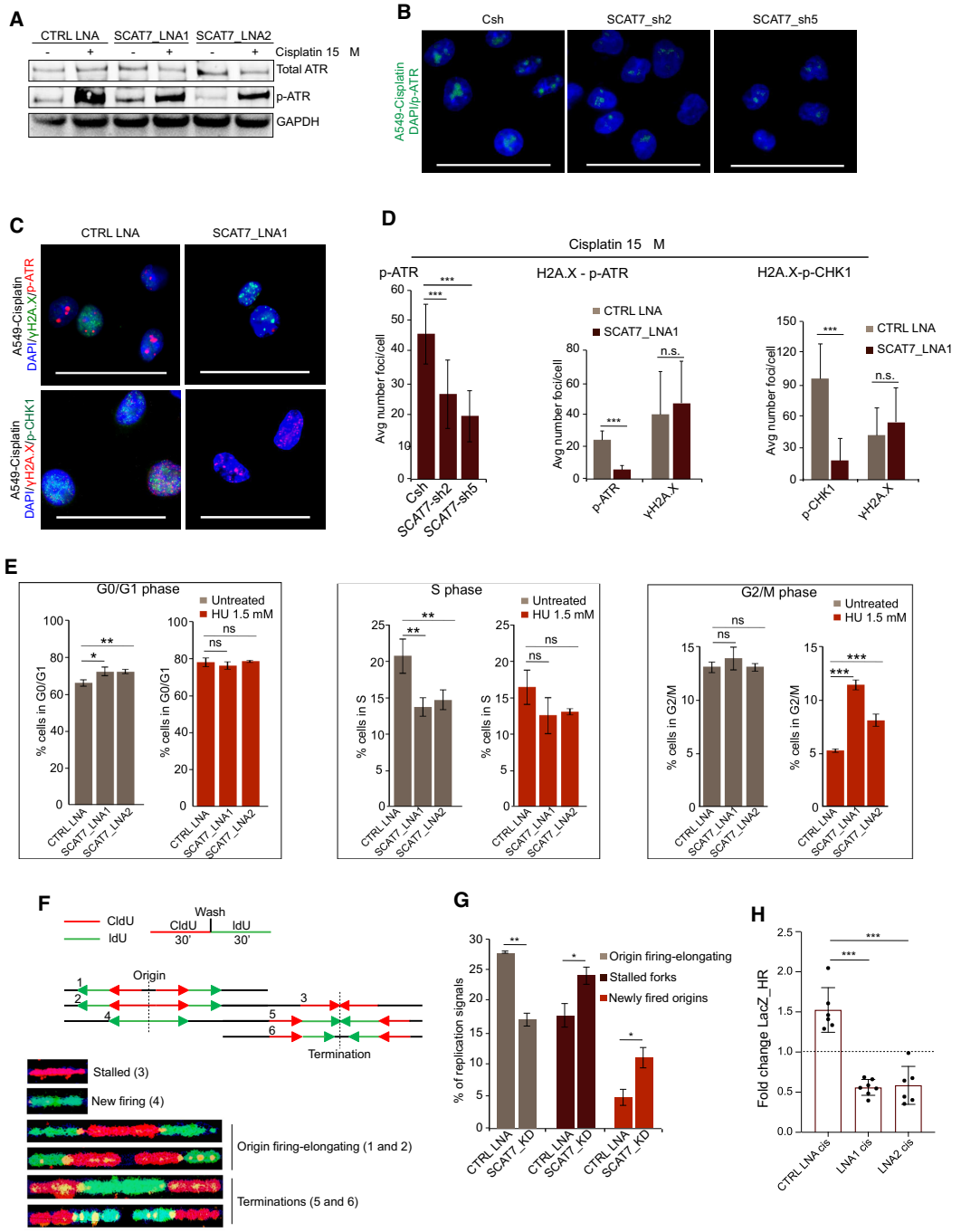

Figure 2. *SCAT7* affects DNA repair and replication. (**A**) Western blot analysis of ATR pathway members with indicated antibodies in A549 cells following *SCAT7* KD. (**B** and **C**) Representative IF images of A549 cells transiently or stably transfected with *SCAT7* targeting GapmeRs or *SCAT7*-sh lentiviral particles following cisplatin treatment. Cells were stained with DAPI (blue) p-ATR (red), γH2A.X and p-CHK-1 (green). Scale bar 50 μm. For (A–C), representative images of at least three independent experiments are shown. (**D**) Quantification of IF experiments depicted in (B) and (C). Data are plotted as average foci number/cell ± SD (*$P \leq 0.05$; **$P = 0.01$ 0.001; ***$P < 0.001$). Significance was derived using two-tailed unpaired Student's *t*-test. (**E**) Graphs depicting the percentage of *SCAT7* depleted A549 cells and GapmeR CTRL in G0/G1, S and G2/M phase, after exposure to 1.5 mM HU for 5 h. Data are plotted as mean ± SD (*$P \leq 0.05$; ** $P = 0.01$ - 0.001; *** $P < 0.001$, unpaired two-sided *t*-test ($n = 3$); (**F**) Sketch depicting the experimental design for DNA fiber assay and the examples of fiber tract types representing the different replication structures. *SCAT7* KD A549 cells and relative control were sequentially pulse-labeled with 0.1 mM CldU and 0.1 mM IdU for 30 min each. Red tracts, CldU; Green tracts, IdU. (**G**) Replication profiles of *SCAT7* KD A549 cells are presented by scoring the percentage of elongating fibers, stalled and newly fired fibers. Five hundred replication signals were scored for each sample. Significance was derived using a two-tailed unpaired Student's *t*-test. Data are plotted as mean ± SD of two independent experiments (*$P \leq 0.05$; **$P = 0.01$ 0.001; *** $P < 0.001$). (**H**) qPCR detection of recombined LacZ sequence (LacZ_HR) in *SCAT7* KD A549 cells with *SCAT7*_LNA1 and LNA2 GapmeRs. *SCAT7* KD cells were transfected with LacZ defective dl-1 and dl-2 HR plasmids for 24 h, followed by 24 h 5 μM cisplatin treatment. Data are presented as Relative Quantity (RQ) of cisplatin-treated samples relative to their specific NT control. Data are represented as average RQ of at least six independent replicates ± SD. Dashed horizontal line = NT set as 1. Significance was retrieved using an unpaired Student's *t*-test (*$P \leq 0.05$; **$P = 0.01$ 0.001; *** $P < 0.001$).

any effect of SCAT7 KD on *ATR* gene expression (data not shown).

Impairment of ATR pathway causes G2/M checkpoint alterations, allowing cancer cells with unrepaired DNA to proceed to mitosis, with deleterious consequences (32). Considering this scenario, we explored the ability of SCAT7 KD cells, which we have previously shown to accumulate in G1/S phase (in accordance with SCAT7 role in S-phase progression), to proceed along the cell cycle in conditions that would activate ATR pathway. To address the latter, we have analyzed the cell cycle profiles of SCAT7 KD cells, where replication stress was induced using hydroxyurea (HU) (Figure 2E). While the progression to the G2-M phase is strongly compromised in CTRL-LNA cells, SCAT7 KD cells seems to have the tendency to progress through the S phase, indicating an impairment of ATR checkpoint kinase activity. Our data suggests that in SCAT7 KD cells ATR signaling is defective and cells are likely to progress to the G2/M phase of the cell cycle when replication stress is chemically induced, thus accumulating unrepaired DNA.

To gain a deeper understanding of the direct role of SCAT7-dependent DNA damage on DNA replication, we analyzed the replication dynamics of SCAT7 KD cells at the single-molecule level by applying the DNA fiber technique. Cells were labeled dually with two consecutive 30-min pulses with the thymidine analogues 5-chloro-2'-deoxyuridine (CldU) and 5-Iodo-2′-deoxyuridine (IdU), followed by analysis of labeled DNA for the identification of nascent replication regions (Figure 2F). We used asynchronous cell populations to avoid any replication artifact and ensure that our observations were due to SCAT7 modulation. The labeling identified six major types of replication signals, as indicated in Figure 2F. Of note, SCAT7 KD cells showed a significant reduction in origin firing and elongation, whereas they exhibited a higher percentage of stalled and newly fired forks (Figure 2G). In the context of replication stress, activated ATR/CHK1 signaling stabilizes the replication fork, preventing new origin firing and facilitating the activation of repair pathways (33,34). This protects cells from further accumulation of stress in undamaged or non-replicating regions (35–37). Therefore, in SCAT7 KD cells, the accumulation of DNA damage could be due to SCAT7 KD-induced fork stalling, while the increase of newly fired forks could be attributed to the inability of the cells with impaired ATR activation to stabilize stalled forks, leading to the activation of dormant origins (38). Based on the connection between ATR function and DNA repair, we evaluated the activation of the main DNA repair pathways HR and NHEJ in SCAT7 KD cells. We analyzed HR efficiency in SCAT7 KD cells, before and after cisplatin treatment. Transient and stable SCAT7 KD cells were co-transfected with two plasmids expressing truncated LacZ, followed by PCR detection of the fused LacZ sequence in cells that undergo HR. While control cells were able to perform HR, this process was significantly impaired in SCAT7 KD cells, as shown by RT-qPCR of the recombined *LacZ* region using primers flanking the recombination site in cisplatin treated cells compared to their respective non-treated controls (Figure 2H and Supplementary Figure S2B), indicating that SCAT7 KD impairs HR. We also tested the levels of NHEJ in SCAT7 KD HN-HeLa NHEJ reporter cell line, after treatment with cisplatin. These cells have a GFP gene disrupted by an intron which is flanked by I-*Sce*I restriction sites. When HN-HeLa cells were transfected with a doxycyclin inducible plasmid containing the enzyme I-*Sce*I, the intron is removed and cells will express GFP as result of successful NHEJ. The ability of HN-HeLa SCAT7 KD cells to perform NHEJ following the induction of I-*Sce*I was unaffected, if not slightly induced, indicating that this repair pathway was not altered in our system (Supplementary Figure S2C and D). In line with this, no consistent changes were observed in the expression of crucial NHEJ partners KU70–80, XRCC4 and Ligase IV, which specifically take part in NHEJ, confirming the functionality of this pathway in SCAT7 KD cells (Supplementary Figure S2E). Collectively, these results suggest that the impairment of ATR signaling observed in SCAT7 KD cells, besides interfering with fork progression, reduces ATR-mediated engagement of the HR pathway, thus disrupting more than one protective mechanism enacted by hyperproliferative cancer cells exposed to cytotoxic drugs.

SCAT7 regulates topoisomerase 1 turnover in a proteasome-dependent manner

Among SCAT7-interacting proteins, a potential candidate for establishing the direct involvement of SCAT7 KD in the formation of DSBs is TOP1. TOP1 is a single strand nicking enzyme acting at the interface between replication and transcription, essential for the resolution of replication/transcription conflicts (39). For proper catalytic unwinding of DNA, TOP1 associates with a transient single-strand DNA intermediate and forms the TOP1–cc). The resolution of the TOP1–cc complex requires the activation of the DDR pathway in an ubiquitin-dependent manner (40–42). Failure of activation of this degradation pathway, as well as the exposure to TOP1 inhibitors like CPT, promote the accumulation of TOP1–cc. This irreversible DNA-bound complex induces stalled replication forks causing activation of the genome surveillance pathway regulated by ATR (43). Morevoer, TOP1–cc cause intrinsic DNA damage when they collide with replication or transcriptional machinery, or when they occur in the vicinity of other DNA lesions (44,45).

Based on the effect of SCAT7 KD on ATR signaling and HR, we sought to explore if and how SCAT7 contributes to this processes through its interaction with TOP1. To start with, we validated the previously obtained ChOP/MS data on SCAT7 interaction with TOP1 with two independent approaches, RNA immunoprecipitation (RIP) (Figure 3A) and SCAT7 ChOP followed by immunobloting (Figure 3B). We then evaluated the contribution of SCAT7 in TOP1 turnover by analyzing TOP1 levels in SCAT7 KD cells treated with CPT, a TOP1 poison which acts at the TOP1–cc complex to stabilize the interaction between TOP1 and DNA, thereby inducing DNA damage and apoptosis. We observed that TOP1 is accumulated in SCAT7 KD cells treated with CPT, indicating that SCAT7 KD affects TOP1 turnover (Figure 3C). To fine map the region of SCAT7 that promotes TOP1 turnover, we overexpressed different constructs containing fragments of the SCAT lncRNA in A549 cells (Figure 3D). As shown in Figure 3E, the in-

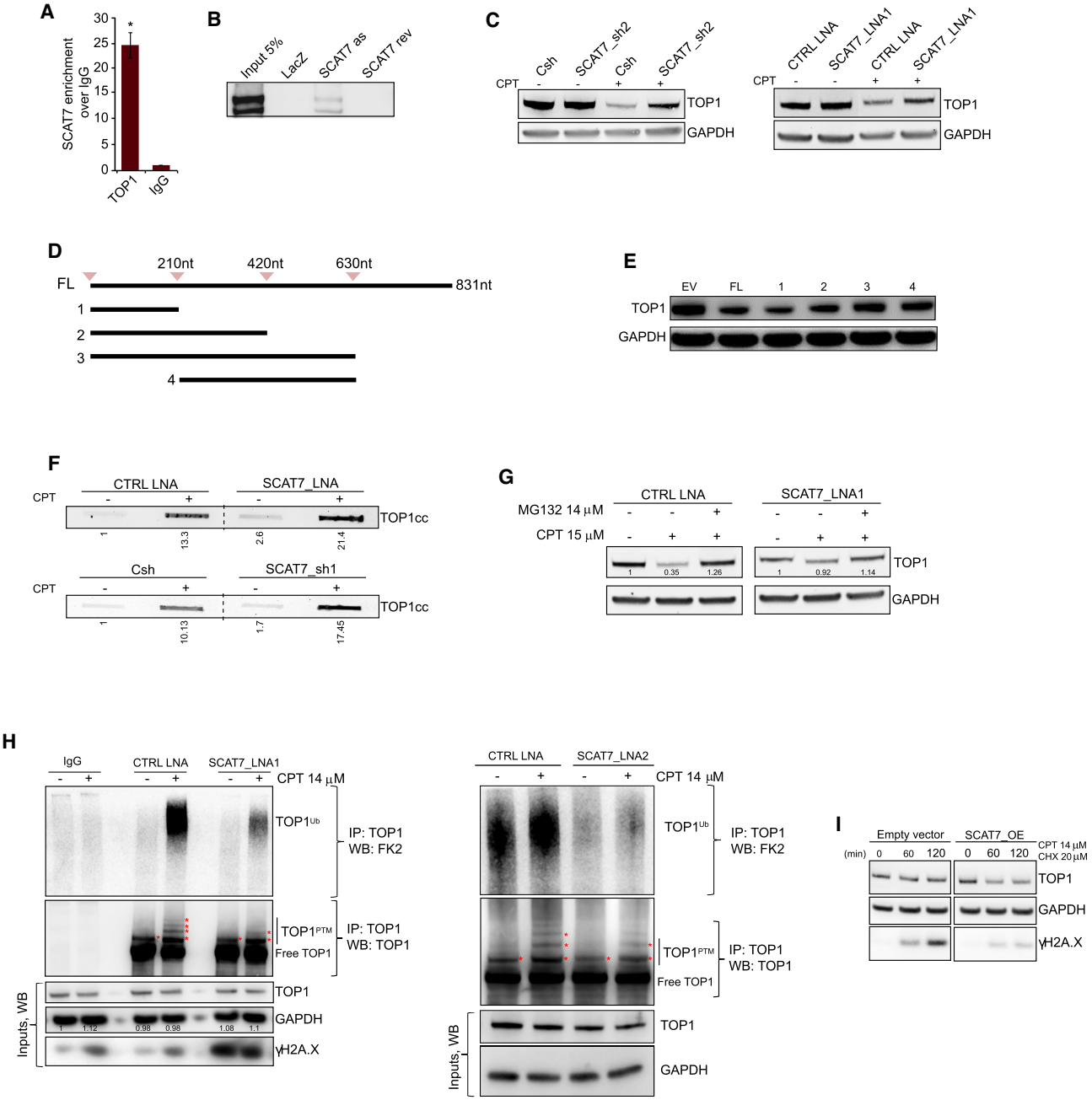

Figure 3. SCAT7 regulates TOP1 turnover. (**A**) RIP followed by RT-qPCR for *SCAT7* using antibodies against TOP1 and IgG. Data are depicted as fold enrichment on IgG control; (**B**) Western blot of *SCAT7*-interacting TOP1 in A549 cells following ChOP using biotinylated antisense probe specific to *SCAT7* (SCAT7 as), sense probe (SCAT7 rev), or LacZ negative probe; (**C**) Western blot of TOP1 in transient and stable *SCAT7* KD A549 cells following 15 μM CPT treatment for 2 h. Immunoblot images are representative of at least three independent experiments; (**D**) Schematic of the different fragments of *SCAT7* transcripts that were inserted into inducible overexpression plasmids; (**E**) Immunoblot of TOP1 in A549 cells transfected with overexpression plasmids containing different fragments of *SCAT7* transcript, as described in Figure 3D, after treating cells with 15 μM CPT for 2 h. (**F**) Immunoblot of TOP1–cc levels on DNA following ICE assay in transient and stable SCAT7 KD A549 cells. TOP1–cc levels were normalized to untreated control; (**G**) Western blot of TOP1 in SCAT7 KD A549 cells following CPT treatment in the presence or absence of MG132 proteasome inhibitor. TOP1 levels were normalized to respective untreated control. Immunoblot image is representative of at least three independent experiments; (**H**) Poly-ubiquitin (pUB) immunoblot of immunoprecipitated TOP1 in A549 cells transfected with two LNA GapmeRs targeting SCAT7, and relative control cells following CPT treatment. pUB levels were normalized with respect to CTRL LNA. Immunoblot for the indicated protein (TOP1, γH2A.X and GAPDH) with input (bottom). IgG was used as specificity controls. Representative images of at least three independent experiments; (**I**) Western blot of SCAT7 overexpressing A549 cells following combined treatment with CPT and Cycloheximide (CHX) in a time course of 2 h. Representative images of at least two independent experiments.

ducible overexpression of the 5'end fragment of *SCAT7* (1–210 nt) efficiently promoted TOP1 turnover. We performed ICE (*in vivo* complex of enzyme) assay on control and SCAT7 KD cells following CPT treatment by isolating genomic DNA under conditions that preserve DNA–protein complexes, followed by immunoblot of the DNA–protein complex with TOP1 antibody. The ICE assay revealed that the majority of accumulated TOP1 in SCAT7 KD cells is trapped in TOP1–cc complexes, and likely contributes to the high level of genotoxic stress (Figure 3F). Since TOP1 turnover is proteasome dependent (42), we tested the possibility that SCAT7 binding to TOP1 facilitates its ubiquitin-dependent degradation. To this end, we evaluated TOP1 levels in SCAT7 KD cells after CPT treatment alone or in the presence of the proteasome inhibitor MG132. Interestingly, TOP1 levels decrease in control cells after 2 h of CPT treatment. However, in SCAT7 KD cells, TOP1 levels were less affected by CPT treatment (Figure 3G). To check whether SCAT7 KD interferes with the ubiquitination of TOP1, we immunoprecipitated TOP1 in control and SCAT7 KD cells. The western blot analysis of immunoprecipitates after treatment with CPT revealed high levels of ubiquitinated TOP1 in control cells. However, TOP1 ubiquitination is strongly impaired in SCAT7 KD cells (Figure 3H). Moreover, TOP1 immunoblotting showed that TOP1 post-translational modifications, marked as asterisks in Figure 3H, are lost upon SCAT7 KD, indicating an involvement of SCAT7 in TOP1 ubiquitination. Further, to support the SCAT7-dependent regulation of TOP1 turnover, we assessed TOP1 half-life in cells differentially expressing SCAT7 in the presence of CPT and cycloheximide (CHX). In this context, cells with reduced protein turnover would have a more stable expression of TOP1 following CHX treatment. Consistent with our previous results, SCAT7-overexpressing cells are more affected in TOP1 turnover after 1- and 2-h co-treatment with CPT and CHX, confirming the role of SCAT7 in regulating TOP1 stability (Figure 3I). In line with our hypothesis that SCAT7 is involved in maintaining genomic stability we also observed a decrease in γH2A.X in SCAT7 overexpression cells (Please see lower panel in Figure 3I). Collectively, these results show that SCAT7 is at a central point in regulating genomic stability through fine-tuning TOP1 turnover.

We postulate that by interacting with TOP1, SCAT7 acts as a TOP1 scaffold to promote its post-translational modifications and turnover. Therefore, SCAT7 abrogation accounts for the induction of intrinsic DNA damage in unperturbed cells as well as cells perturbed with cytotoxic-agents.

SCAT7 downregulation in A549/cDDP phenocopies the effect of cisplatin in parental A549 cells

Cisplatin is one of the first line treatments for non-small cell lung cancer (46). Nucleotide excision repair and HR are the main repair pathways activated by cancer cells in response to cisplatin (47–50). Given our *in vitro* data, showing a simultaneous impairment of HR ability, ATR pathway activation and TOP1 turnover in SCAT7 KD A549 cells, we sought to investigate the possible role of SCAT7 in cisplatin resistance through the disruption of these survival pathways. To this end, we have generated cisplatin-resistant A549 cells (A549/cDDP) from the parental cell line. A549/cDDP cells showed mesenchymal morphology with slightly increased size and spindle-shaped appearance. Consistent with morphology, A549/cDDP cells exhibit an epithelial-mesenchymal transition profile, with downregulation of epithelial marker E-cadherin and upregulation of the mesenchymal marker vimentin (Figure 4A). We performed RNA-seq of A549/cDDP cells and parental A549 to identify the molecular pathways affected in resistant cells. Interestingly, pathways enriched for upregulated genes in A549/cDDP cells showed significant overrepresentation of extracellular matrix organization functions. Pathways from downregulated genes were mostly related to the regulation of cell cycle and DNA replication (Figure 4B and Supplementary Table S3). This indicates that resistant cells differently regulate their cell cycle compared to the parental cells. On the other hand, upregulation of collagen genes might be involved in the acquisition of malignant and metastatic phenotypes. Given that *SCAT7* is activated by cisplatin treatment, we sought to explore a possible role of SCAT7 in mitigating the cisplatin resistance phenotype. However, in cDDP cells SCAT7 levels were similar to the non-treated wild-type (WT) A549 cells (Figure 4C), therefore we assumed that SCAT7 overexpression is not important in establishing cDDP resistance. However, its basal expression could be critical for the maintenance of the resistant status. To this end, we downregulated SCAT7 in A549/cDDP cells. MTT analysis revealed that SCAT7 KD significantly affected the proliferation of A549/cDDP cells; however, we did not observe an additive effect of SCAT7 KD and cisplatin treatment as in sensitive cells (Figure 4D). We considered this phenotype of particular interest and worth further exploration, in the light of possible therapeutic consideration.

To evaluate if SCAT7 could interfere with cisplatin resistance in cDDP cells, we performed RNA-seq in A549/cDDP cells treated either with cisplatin or SCAT7 LNA GapmeRs. RNA-seq analyses confirmed the acquired resistance of A549/cDDP cells, as we did not observe any significantly enriched molecular pathways in response to cisplatin treatment (Supplementary Table S3). On the contrary, cisplatin treatment in A549 WT cells induced global transcriptional modulation, reflected by the significant enrichment of DNA repair, checkpoints activation and cell cycle-related pathways (Figure 4E and Supplementary Table S3). Of note, *SCAT7* depletion in A549/cDDP cells resulted in the dysregulation of DNA replication, telomere maintenance, and cell cycle-related pathways. Interestingly, we observed many overlapping differentially expressed transcripts between cisplatin-treated WT A549 cells and SCAT7 KD cDDP cells. (Figure 4E and F; Supplementary Table S3). These results indicate that even if SCAT7 is not overexpressed in cDDP-A549 compared to WT cells, its upregulation during cisplatin treatment is required for cell survival and SCAT7 KD in cDDP cells affects the same cell survival-associated pathways, indicating that SCAT7 basal expression is critical for maintenance of the resistance phenotype.

We next explored the therapeutic potential of SCAT7 targeting in cisplatin-resistant tumors. Toward this, we generated Balb/c nude xenografts by subcutaneous injection of

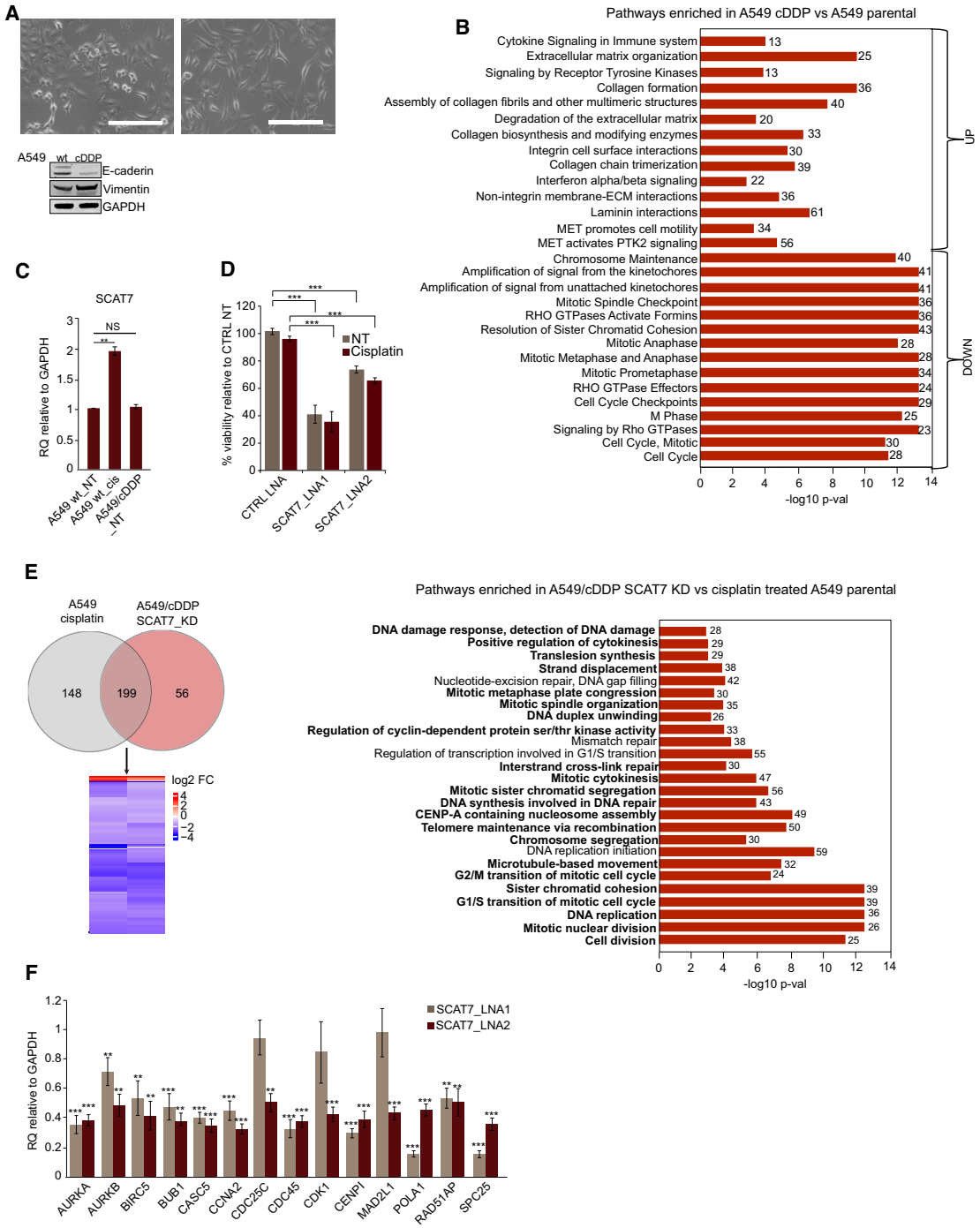

Figure 4. SCAT7 depletion in A549/cDDP cells recapitulates the pathways activated by cisplatin in parental cells. (**A**) Phase contrast microscope images of wildtype A549 (left) and A549/cDDP (right) cells. Western blots by the images show the indicated epithelial/mesenchymal markers in A549 and A549/cDDP cells; (**B**) Biological pathways enriched in A549/cDDP cells relative to the parental A549 cells. Graph indicates -log10 FDR for each pathway, the numbers are the percentage of genes enriched from each process. Significance was obtained using *P*-value ≤ 0.05; (**C**) MTT assay on SCAT7 KD A549/cDDP cells before and after treatment with cisplatin at the IC50 for parental cells. NT refers to non-treated. Data are represented as percentage compared to untreated cells transfected with control LNA. Mean values of at least three independent experiments are shown and statistical significance was derived using a two-tailed unpaired Student's *t*-test. Data are plotted as mean ± SD (*$P \leq 0.05$; **$P = 0.01$ 0.001; ***$P < 0.001$); (**D**) *SCAT7* expression in A549 WT cells ± 15 μM cisplatin and cDDP cells grown in 15 μM cisplatin shows that SCAT7 is not induced in resistant cells. Data are plotted as mean ± SD of three independent replicates. Statistical significance was derived using a two-tailed unpaired Student's *t*-test (*$P \leq 0.05$; **$P = 0.01$ 0.001; ***$P < 0.001$); (**E**) Left: the Venn diagram shows the common genes in the overlapping pathways between cisplatin-treated A549 and SCAT7 KD A549/cDDP cells, and heatmap depicts the log2 FC for the 199 common genes in the two sets of samples. Right: biological pathways enriched in SCAT7 KD A549/cDDP cells. Pathways in bold are common to the ones enriched in parental A549 cells after cisplatin treatment. Graph indicates -log10 FDR for each pathway, the numbers represent the percentage of genes enriched from each process. (**F**) qPCR validation of *SCAT7* KD A549/cDDP sequencing data using two independent LNA GapmeRs. Experiments were performed in triplicate and data are plotted as mean ± SD.

either WT A549 or A549/cDDP cells to evaluate the response of resistant tumors to cisplatin therapy in association with SCAT7 downregulation. When tumors became measurable, we started a therapeutic regimen based on the subcutaneous peritumoral injection of LNAs and cisplatin in combination (cisplatin and SCAT7 LNA or cisplatin and CTRL LNA) or individually (Figure 5A). As expected, tumor growth of WT A549-derived xenografts was most affected by the combination treatment of cisplatin/SCAT7 LNA, compared to cisplatin/CTRL LNA or cisplatin alone (Figure 5B). In A549/cDDP xenografts, CTRL LNA alone or in combination with cisplatin did not affect tumor growth, while we observed a significant tumor inhibition in A549/cDDP xenografts treated with SCAT7 LNA (Figure 5C and D). Moreover, cisplatin treatment had no effect on the cDDP cell growth both *in vitro* and *in vivo* (Figures 4C and 5D), indicating that SCAT7 KD alone is responsible for the reduced tumor growth of A549/cDDP cells. When it comes to side effects, cisplatin-treated mice developed dry skin, loss of weight, nervous behavior as well as tail ulcerations, requiring early termination of the experiment, whereas such effects were not observed in the LNA only treated group. Thus, targeting SCAT7 could be explored as a novel therapeutic approach for cancers that develop resistance to cisplatin, avoiding the toxic effects of the drug.

DISCUSSION

LncRNAs have been associated with most cancer-related hallmarks including proliferation, apoptosis, cell cycle regulation and senescence (51). Recent studies have identified a new exciting role of lncRNAs in the maintenance of genome stability (52–54), as a growing number of lncRNAs has been shown to be directly regulated by the main keepers of genome integrity (55,56). Genomic instability can lead to cancer and degenerative diseases, and eukaryotic cells have developed multiple molecular mechanisms to sense DNA damage and activate reparatory responses to grant cell survival. This concept has been exploited in developing cancer therapies causing DNA damage and taking advantage of the inability of cancer cells to repair it, forcing them into apoptosis. In this scenario lncRNAs stand out as versatile regulatory players of most of the physiological and pathological processes in eukaryotic cells. Previous investigations have implicated several lncRNAs in DDR in a p53-independent or dependent fashion (7–11). However, the mechanisms by which the loss of a particular lncRNA leads to DNA damage are not fully understood.

We have identified the lncRNA SCAT7 (ELF3-AS), with preferential nuclear localization, highly expressed in the cell cycle S-phase, as an oncogenic driver overexpressed in multiple cancers (13). While performing functional screenings for the identification of SCAT7-dependent molecular pathways, we noticed that several of its protein interactors are nuclear proteins with key functions in maintaining DNA stability, as well as repair proteins and chromatin remodelers, suggesting a potential role for SCAT7 in maintaining genomic integrity. The hypothesis that SCAT7 might have a role in genome stability was further reinforced by its strong, but selective, activation following treatment with replication inhibitors like cisplatin and CPT, but not other drugs like etoposide, doxorubicin and nutlin-3a. At the same time, its depletion activates transcriptional events similar to drug-induced DNA damage.

To dissect the molecular mechanisms of SCAT7-dependent DNA damage, we analyzed its role in promoting faithful DNA replication, its ability to activate the S-phase cell cycle checkpoints and efficient DNA repair (57). While NHEJ, which acts throughout the cell cycle, is the preferred repair mechanism occurring prior to DNA replication (58), cells turn on the error-free HR pathway for DNA damage occurring during the S-phase (59,60). While NHEJ remains unaffected in SCAT7 KD cells, SCAT7 downregulation affects HR, most likely through the impairment of the ATR signaling pathway. One way the impairment of SCAT7 interferes with ATR activation could be through the multiple cell signaling cascades that we have previously identified to be disrupted by SCAT7 downregulation. For example, one of the many factors activating ATR pathway during HU induced replication stress is ERK, which induces formation of ATR nuclear foci after cytotoxic induction of replication stress (61). We have previously shown that SCAT7 depletion leads to impairment of ERK phosphorylation in different cancer cell types, including A549 (13), thereby affecting ATR pathway.

ATR kinase is canonically activated in response to DNA damage, ssDNA accumulation during replication (62) and increased fork stalling induced by TOP1–cc increase when cells are challenged with TOP1 poisons. Given the link between SCAT7 and ATR signaling, it is important to underline two main points raised in our study: (i) SCAT7 KD increased fork stalling and new fork firing in an attempt to complete DNA replication, during cisplatin treatment. This in turn explains the accumulation of the unrepaired DSBs in these cells, compared to cells expressing SCAT7 normally. (ii) On the other hand, by focusing on SCAT7-TOP1 interaction, we hypothesize a causal connection with intrinsic DNA damage onset. TOP1 acts to reduce DNA supercoiling during replication by covalently interacting with 3' ssDNA. This interaction is transient and tightly regulated by the presence of a finely tuned degradation pathway that involves, among other factors, the ubiquitin-dependent proteasome machinery (34). Failure to degrade these transient complexes leads to the persistence of TOP1–cc complexes, representing an obstacle to replication fork progression and resulting in DSBs. In the context of SCAT7 KD, impaired ATR signaling is concomitant to a reduced TOP1 turnover. These cells suffer alterations of two major genomic surveillance mediators, whose dysfunction is intimately connected to cell death. We therefore conclude that in SCAT7 KD cells, failure of TOP1 degradation accounts for the induction of DNA damage. Furthermore, the interference with HR through the impairment of ATR functions accounts for the inability of SCAT7 KD cells to faithfully repair the induced damage, resulting in exacerbated γH2A.X accumulation, leading to apoptosis.

Multiple cellular mechanisms are involved in the acquisition of resistance to cisplatin-based therapies, (63,64). Since HR is the main mechanism applied for the repair of CDDP based lesions (65), targeting HR pathway is considered a promising therapeutic option in the treatment of CDDP resistant cancers (66). Despite the development of highly spe-

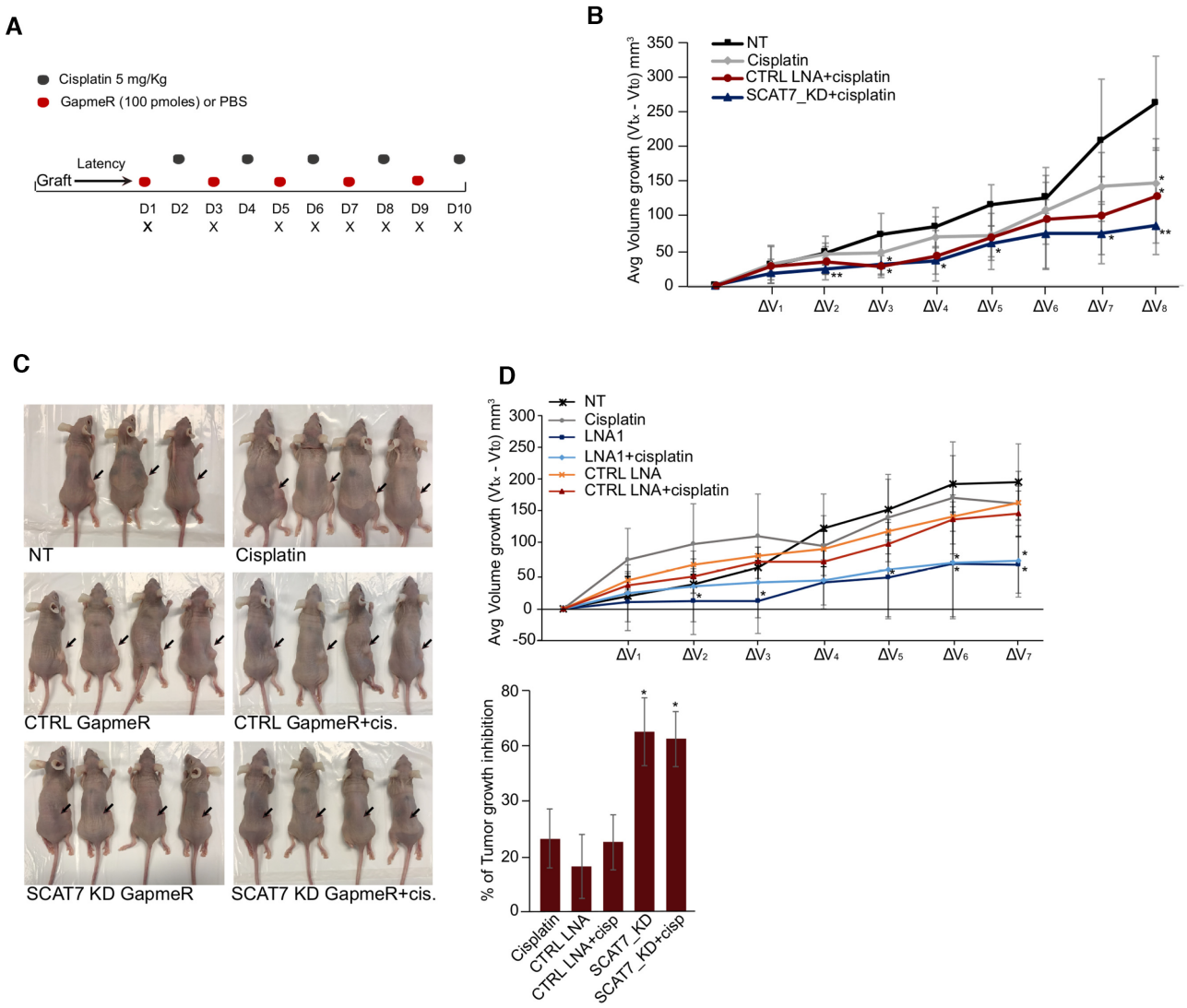

Figure 5. SCAT7 KD reduces tumor growth in cisplatin resistant xenograft models of LUAD. (**A**) Graphical representation of the therapeutic regimen applied to the A549 mice xenografts. X indicates the time points when tumors where measured. (**B**) Graph showing the average tumor growth of parental A549 xenografts (ΔV = Vtx-Vt0) treated with cisplatin, or CTRL or *SCAT7* LNA-GapmeRs in combination with cisplatin, and non-treated controls. (**C**) Pictures of Balb/c nude mice A549/cDDP xenografts at day of dissection. Arrows indicate the subcutaneous tumor. (**D**) Top: Graph showing the average tumor growth of A549/cDDP xenografts depicted in C) treated with control or SCAT7 LNA-GapmeRs alone or in combination with cisplatin, cisplatin only and non-treated controls. Significance was derived using a two-tailed unpaired Student's *t*-test. Bottom: Tumor growth inhibition (TGI) for A549/cDDP subcutaneous Balb/c nude xenografts depicted in (C). For (B) and (D), average tumor growth was calculated with the formula ΔV = Vtx-Vt0. Data are plotted as mean ± SD (*$P \leq 0.05$; **$P = 0.01$ 0.001; *** $P < 0.001$).

cific inhibitors for some proteins involved in HR has paved the road to the identification of targeted therapies for this pathway (67,68), it is worth considering that several HR modulators are implicated in a plethora of essential and physiological functions (69–71), therefore their inhibition could still potentially elicit toxicity in many instances (72). Considering SCAT7 role in HR modulation and that there were no noticeable side effects in our CDDP xenograft models, we believe that SCAT7 KD could be further explored as a means of inhibiting HR in cancer cells. Interestingly, SCAT7 KD in cisplatin-resistant cells can restore the pathways that are activated in sensitive cells following cisplatin treatment. This is in accordance with its critical role in the maintenance of genomic integrity, and with our hypothesis that *SCAT7* depletion mimics the biological effects of cisplatin treatment. Moreover, our LNA-ASOs based therapeutic intervention successfully reduced the tumor growth of cisplatin-resistant tumors in xenograft models of LUAD. Taken together, these results suggest that SCAT7 targeted therapy could be a potential option for hard-to-treat cancers.

DATA AVAILABILITY

The data associated with this publication have been deposited in GEO: GSE116192.

https://www.ncbi.nlm.nih.gov/geo/query/acc.cgi?acc=GSE116192.

SUPPLEMENTARY DATA

Supplementary Data are available at NAR Cancer Online.

ACKNOWLEDGEMENTS

The computations for the dataset used in the current study were performed on resources provided by Uppsala Multidisciplinary Center for Advanced Computational Science (UPPMAX) high-performance computing (HPC) which is part of Swedish National Infrastructure for Computing (SNIC).

Author contributions: C.K. and L.S. conceptualized the research, designed experiments and wrote the paper. L.S. performed all drug treatments and functional analysis, generated and characterized A549/cDDP cells, performed all western blots, some IF, network analysis on *SCAT7* protein interactors and pathway analysis on sequencing data, TOP1 turnover experiments in *SCAT7* KD cells, all xenograft experiments. M.M.A. performed IF, ChOP-western blot, western blots, helped in conceptual and experimental design. S.R. performed OE experiments and cychloheximide experiment. S.M. performed western blots on SCAT7 overexpression and OE experiments, S.T.K. helped with RNA-seq data analysis and performed the GO analysis; L.S., C.K., M.M.A., S.R., S.M., S.T.K. and M.H. performed data analysis/interepretation.

FUNDING

Knut and Alice Wallenberg Foundation [KAW2014.0057]; Swedish Foundation for Strategic Research [RB13–0204]; Cancerfonden [CAN2018/591]; Swedish Research Council [2017–02834]; Barncancerfonden [PR2018–0090]; Ingabritt Och Arne Lundbergs forskningsstiftelse; LUA/ALF (to C.K.); Assar Gabrielssons Foundation AG Fond [FB-17 to L.S.].

Conflict of interest statement. C.K., L.S., M.M.A. and S.T.K. have have been granted a patent titled 'Long non-coding RNA in Cancer' related to findings from the current manuscript. PCT/EP2018/065210. USA patent application No. 16/620,700 and EPO application No. 18730745.9.

REFERENCES

1. Rothkamm,K., Barnard,S., Moquet,J., Ellender,M., Rana,Z. and Burdak-Rothkamm,S. (2015) DNA damage foci: Meaning and significance. *Environ. Mol. Mutagen.*, **56**, 491–504.
2. Lempiainen,H. and Halazonetis,T.D. (2009) Emerging common themes in regulation of PIKKs and PI3Ks. *EMBO J.*, **28**, 3067–3073.
3. Jackson,S.P. and Bartek,J. (2009) The DNA-damage response in human biology and disease. *Nature*, **461**, 1071–1078.
4. Brandsma,I. and Gent,D.C. (2012) Pathway choice in DNA double strand break repair: observations of a balancing act. *Genome Integr.*, **3**, 9.
5. Zeman,M.K. and Cimprich,K.A. (2014) Causes and consequences of replication stress. *Nat. Cell Biol.*, **16**, 2–9.
6. Cimprich,K.A. and Cortez,D. (2008) ATR: an essential regulator of genome integrity. *Nat. Rev. Mol. Cell Biol.*, **9**, 616–627.
7. Sharma,V., Khurana,S., Kubben,N., Abdelmohsen,K., Oberdoerffer,P., Gorospe,M. and Misteli,T. (2015) A BRCA1-interacting lncRNA regulates homologous recombination. *EMBO Rep.*, **16**, 1520–1534.
8. Zhang,Y., He,Q., Hu,Z., Feng,Y., Fan,L., Tang,Z., Yuan,J., Shan,W., Li,C., Hu,X. *et al.* (2016) Long noncoding RNA LINP1 regulates repair of DNA double-strand breaks in triple-negative breast cancer. *Nat. Struct. Mol. Biol.*, **23**, 522–530.
9. Hu,W.L., Jin,L., Xu,A., Wang,Y.F., Thorne,R.F., Zhang,X.D. and Wu,M. (2018) GUARDIN is a p53-responsive long non-coding RNA that is essential for genomic stability. *Nat. Cell Biol.*, **20**, 492–502.
10. Adriaens,C., Standaert,L., Barra,J., Latil,M., Verfaillie,A., Kalev,P., Boeckx,B., Wijnhoven,P.W., Radaelli,E., Vermi,W. *et al.* (2016) p53 induces formation of NEAT1 lncRNA-containing paraspeckles that modulate replication stress response and chemosensitivity. *Nat. Med.*, **22**, 861–868.
11. Diaz-Lagares,A., Crujeiras,A.B., Lopez-Serra,P., Soler,M., Setien,F., Goyal,A., Sandoval,J., Hashimoto,Y., Martinez-Cardus,A., Gomez,A. *et al.* (2016) Epigenetic inactivation of the p53-induced long noncoding RNA TP53 target 1 in human cancer. *Proc. Natl Acad. Sci. U.S.A.*, **113**, E7535–E7544.
12. Subhash,S. and Kanduri,C. (2016) GeneSCF: a real-time based functional enrichment tool with support for multiple organisms. *BMC Bioinformatics*, **17**, 365.
13. Ali,M.M., Akhade,V.S., Kosalai,S.T., Subhash,S., Statello,L., Meryet-Figuiere,M., Abrahamsson,J., Mondal,T. and Kanduri,C. (2018) PAN-cancer analysis of S-phase enriched lncRNAs identifies oncogenic drivers and biomarkers. *Nat. Commun.*, **9**, 883.
14. Shannon,P., Markiel,A., Ozier,O., Baliga,N.S., Wang,J.T., Ramage,D., Amin,N., Schwikowski,B. and Ideker,T. (2003) Cytoscape: a software environment for integrated models of biomolecular interaction networks. *Genome Res.*, **13**, 2498–2504.
15. Gatchalian,J., Malik,S., Ho,J., Lee,D.S., Kelso,T.W.R., Shokhirev,M.N., Dixon,J.R. and Hargreaves,D.C. (2018) A non-canonical BRD9-containing BAF chromatin remodeling complex regulates naive pluripotency in mouse embryonic stem cells. *Nat. Commun.*, **9**, 5139.
16. Davis,A.J., Chen,B.P. and Chen,D.J. (2014) DNA-PK: a dynamic enzyme in a versatile DSB repair pathway. *DNA Repair (Amst.)*, **17**, 21–29.
17. Pommier,Y., Barcelo,J.M., Rao,V.A., Sordet,O., Jobson,A.G., Thibaut,L., Miao,Z.H., Seiler,J.A., Zhang,H., Marchand,C. *et al.* (2006) Repair of topoisomerase I-mediated DNA damage. *Prog. Nucleic Acid Res. Mol. Biol.*, **81**, 179–229.
18. Rajesh,C., Baker,D.K., Pierce,A.J. and Pittman,D.L. (2011) The splicing-factor related protein SFPQ/PSF interacts with RAD51D and is necessary for homology-directed repair and sister chromatid cohesion. *Nucleic Acids Res.*, **39**, 132–145.
19. Robison,B., Guacci,V. and Koshland,D. (2018) A role for the Smc3 hinge domain in the maintenance of sister chromatid cohesion. *Mol. Biol. Cell*, **29**, 339–355.
20. Li,T., Chen,L., Cheng,J., Dai,J., Huang,Y., Zhang,J., Liu,Z., Li,A., Li,N., Wang,H. *et al.* (2016) SUMOylated NKAP is essential for chromosome alignment by anchoring CENP-E to kinetochores. *Nat. Commun.*, **7**, 12969.
21. Chibi,M., Meyer,M., Skepu,A., DJ,G.R., Moolman-Smook,J.C. and Pugh,D.J. (2008) RBBP6 interacts with multifunctional protein YB-1 through its RING finger domain, leading to ubiquitination and proteosomal degradation of YB-1. *J. Mol. Biol.*, **384**, 908–916.
22. Mouysset,J., Gilberto,S., Meier,M.G., Lampert,F., Belwal,M., Meraldi,P. and Peter,M. (2015) CRL4(RBBP7) is required for efficient CENP-A deposition at centromeres. *J. Cell Sci.*, **128**, 1732–1745.
23. Zhang,Z., Yang,H. and Wang,H. (2014) The histone H2A deubiquitinase USP16 interacts with HERC2 and fine-tunes cellular response to DNA damage. *J. Biol. Chem.*, **289**, 32883–32894.
24. Maere,S., Heymans,K. and Kuiper,M. (2005) BiNGO: a Cytoscape plugin to assess overrepresentation of gene ontology categories in biological networks. *Bioinformatics*, **21**, 3448–3449.
25. Munschauer,M., Nguyen,C.T., Sirokman,K., Hartigan,C.R., Hogstrom,L., Engreitz,J.M., Ulirsch,J.C., Fulco,C.P., Subramanian,V., Chen,J. *et al.* (2018) The NORAD lncRNA assembles a topoisomerase complex critical for genome stability. *Nature*, **561**, 132–136.
26. Karimian,A., Ahmadi,Y. and Yousefi,B. (2016) Multiple functions of p21 in cell cycle, apoptosis and transcriptional regulation after DNA damage. *DNA Repair (Amst.)*, **42**, 63–71.
27. Xu,Y. and Her,C. (2015) Inhibition of topoisomerase (DNA) I (TOP1): DNA damage repair and anticancer therapy. *Biomolecules*, **5**, 1652–1670.

28. Moynahan,M.E. and Jasin,M. (2010) Mitotic homologous recombination maintains genomic stability and suppresses tumorigenesis. *Nat. Rev. Mol. Cell Biol.*, **11**, 196–207.
29. Buisson,R., Niraj,J., Rodrigue,A., Ho,C.K., Kreuzer,J., Foo,T.K., Hardy,E.J., Dellaire,G., Haas,W., Xia,B. *et al.* (2017) Coupling of homologous recombination and the checkpoint by ATR. *Mol. Cell*, **65**, 336–346.
30. Kim,D., Liu,Y., Oberly,S., Freire,R. and Smolka,M.B. (2018) ATR-mediated proteome remodeling is a major determinant of homologous recombination capacity in cancer cells. *Nucleic Acids Res.*, **46**, 8311–8325.
31. Yazinski,S.A., Comaills,V., Buisson,R., Genois,M.M., Nguyen,H.D., Ho,C.K., Todorova Kwan,T., Morris,R., Lauffer,S., Nussenzweig,A. *et al.* (2017) ATR inhibition disrupts rewired homologous recombination and fork protection pathways in PARP inhibitor-resistant BRCA-deficient cancer cells. *Genes Dev.*, **31**, 318–332.
32. Toledo,L.I., Altmeyer,M., Rask,M.B., Lukas,C., Larsen,D.H., Povlsen,L.K., Bekker-Jensen,S., Mailand,N., Bartek,J. and Lukas,J. (2013) ATR prohibits replication catastrophe by preventing global exhaustion of RPA. *Cell*, **155**, 1088–1103.
33. Couch,F.B., Bansbach,C.E., Driscoll,R., Luzwick,J.W., Glick,G.G., Betous,R., Carroll,C.M., Jung,S.Y., Qin,J., Cimprich,K.A. *et al.* (2013) ATR phosphorylates SMARCAL1 to prevent replication fork collapse. *Genes Dev.*, **27**, 1610–1623.
34. Liao,H., Ji,F., Helleday,T. and Ying,S. (2018) Mechanisms for stalled replication fork stabilization: new targets for synthetic lethality strategies in cancer treatments. *EMBO Rep.*, **19**, e46263.
35. Iyer,D.R. and Rhind,N. (2017) Replication fork slowing and stalling are distinct, checkpoint-independent consequences of replicating damaged DNA. *PLos Genet.*, **13**, e1006958.
36. Yekezare,M., Gomez-Gonzalez,B. and Diffley,J.F. (2013) Controlling DNA replication origins in response to DNA damage - inhibit globally, activate locally. *J. Cell Sci.*, **126**, 1297–1306.
37. Shechter,D., Costanzo,V. and Gautier,J. (2004) ATR and ATM regulate the timing of DNA replication origin firing. *Nat. Cell Biol.*, **6**, 648–655.
38. Ge,X.Q. and Blow,J.J. (2010) Chk1 inhibits replication factory activation but allows dormant origin firing in existing factories. *J. Cell Biol.*, **191**, 1285–1297.
39. Jazayeri,A., Falck,J., Lukas,C., Bartek,J., Smith,G.C., Lukas,J. and Jackson,S.P. (2006) ATM- and cell cycle-dependent regulation of ATR in response to DNA double-strand breaks. *Nat. Cell Biol.*, **8**, 37–45.
40. Alagoz,M., Chiang,S.C., Sharma,A. and El-Khamisy,S.F. (2013) ATM deficiency results in accumulation of DNA-topoisomerase I covalent intermediates in neural cells. *PLoS One*, **8**, e58239.
41. Das,B.B., Antony,S., Gupta,S., Dexheimer,T.S., Redon,C.E., Garfield,S., Shiloh,Y. and Pommier,Y. (2009) Optimal function of the DNA repair enzyme TDP1 requires its phosphorylation by ATM and/or DNA-PK. *EMBO J.*, **28**, 3667–3680.
42. Katyal,S., Lee,Y., Nitiss,K.C., Downing,S.M., Li,Y., Shimada,M., Zhao,J., Russell,H.R., Petrini,J.H., Nitiss,J.L. *et al.* (2014) Aberrant topoisomerase-1 DNA lesions are pathogenic in neurodegenerative genome instability syndromes. *Nat. Neurosci.*, **17**, 813–821.
43. Garcia-Muse,T. and Aguilera,A. (2016) Transcription-replication conflicts: how they occur and how they are resolved. *Nat. Rev. Mol. Cell Biol.*, **17**, 553–563.
44. Lin,C.P., Ban,Y., Lyu,Y.L., Desai,S.D. and Liu,L.F. (2008) A ubiquitin-proteasome pathway for the repair of topoisomerase I-DNA covalent complexes. *J. Biol. Chem.*, **283**, 21074–21083.
45. Hsiang,Y.H., Lihou,M.G. and Liu,L.F. (1989) Arrest of replication forks by drug-stabilized topoisomerase I-DNA cleavable complexes as a mechanism of cell killing by camptothecin. *Cancer Res.*, **49**, 5077–5082.
46. Fennell,D.A., Summers,Y., Cadranel,J., Benepal,T., Christoph,D.C., Lal,R., Das,M., Maxwell,F., Visseren-Grul,C. and Ferry,D. (2016) Cisplatin in the modern era: the backbone of first-line chemotherapy for non-small cell lung cancer. *Cancer Treat. Rev.*, **44**, 42–50.
47. Galluzzi,L., Vitale,I., Michels,J., Brenner,C., Szabadkai,G., Harel-Bellan,A., Castedo,M. and Kroemer,G. (2014) Systems biology of cisplatin resistance: past, present and future. *Cell Death. Dis.*, **5**, e1257.
48. Su,W.P., Hsu,S.H., Wu,C.K., Chang,S.B., Lin,Y.J., Yang,W.B., Hung,J.J., Chiu,W.T., Tzeng,S.F., Tseng,Y.L. *et al.* (2014) Chronic treatment with cisplatin induces replication-dependent sister chromatid recombination to confer cisplatin-resistant phenotype in nasopharyngeal carcinoma. *Oncotarget*, **5**, 6323–6337.
49. Oliver,T.G., Mercer,K.L., Sayles,L.C., Burke,J.R., Mendus,D., Lovejoy,K.S., Cheng,M.H., Subramanian,A., Mu,D., Powers,S. *et al.* (2010) Chronic cisplatin treatment promotes enhanced damage repair and tumor progression in a mouse model of lung cancer. *Genes Dev.*, **24**, 837–852.
50. Wang,Q.E., Milum,K., Han,C., Huang,Y.W., Wani,G., Thomale,J. and Wani,A.A. (2011) Differential contributory roles of nucleotide excision and homologous recombination repair for enhancing cisplatin sensitivity in human ovarian cancer cells. *Mol. Cancer*, **10**, 24.
51. Schmitt,A.M. and Chang,H.Y. (2016) Long noncoding RNAs in cancer pathways. *Cancer Cell*, **29**, 452–463.
52. Khanduja,J.S., Calvo,I.A., Joh,R.I., Hill,I.T. and Motamedi,M. (2016) Nuclear noncoding RNAs and genome stability. *Mol. Cell*, **63**, 7–20.
53. Lee,S., Kopp,F., Chang,T.C., Sataluri,A., Chen,B., Sivakumar,S., Yu,H., Xie,Y. and Mendell,J.T. (2016) Noncoding RNA NORAD regulates genomic stability by sequestering PUMILIO proteins. *Cell*, **164**, 69–80.
54. Su,M., Wang,H., Wang,W., Wang,Y., Ouyang,L., Pan,C., Xia,L., Cao,D. and Liao,Q. (2018) LncRNAs in DNA damage response and repair in cancer cells. *Acta Biochim. Biophys. Sin. (Shanghai)*, **50**, 433–439.
55. Sanchez,Y., Segura,V., Marin-Bejar,O., Athie,A., Marchese,F.P., Gonzalez,J., Bujanda,L., Guo,S., Matheu,A. and Huarte,M. (2014) Genome-wide analysis of the human p53 transcriptional network unveils a lncRNA tumour suppressor signature. *Nat. Commun.*, **5**, 5812.
56. Montes,M. and Lund,A.H. (2016) Emerging roles of lncRNAs in senescence. *FEBS J.*, **283**, 2414–2426.
57. Jossen,R. and Bermejo,R. (2013) The DNA damage checkpoint response to replication stress: a game of forks. *Front. Genet*, **4**, 26.
58. Symington,L.S. and Gautier,J. (2011) Double-strand break end resection and repair pathway choice. *Annu. Rev. Genet.*, **45**, 247–271.
59. Saleh-Gohari,N. and Helleday,T. (2004) Conservative homologous recombination preferentially repairs DNA double-strand breaks in the S phase of the cell cycle in human cells. *Nucleic Acids Res.*, **32**, 3683–3688.
60. Karanam,K., Kafri,R., Loewer,A. and Lahav,G. (2012) Quantitative live cell imaging reveals a gradual shift between DNA repair mechanisms and a maximal use of HR in mid S phase. *Mol. Cell*, **47**, 320–329.
61. Wu,D., Chen,B., Parihar,K., He,L., Fan,C., Zhang,J., Liu,L., Gillis,A., Bruce,A., Kapoor,A. *et al.* (2006) ERK activity facilitates activation of the S-phase DNA damage checkpoint by modulating ATR function. *Oncogene*, **25**, 1153–1164.
62. Schwab,R.A., Blackford,A.N. and Niedzwiedz,W. (2010) ATR activation and replication fork restart are defective in FANCM-deficient cells. *EMBO J.*, **29**, 806–818.
63. Zaal,E.A. and Berkers,C.R. (2018) The influence of metabolism on drug response in cancer. *Front. Oncol.*, **8**, 500.
64. Chen,S.H. and Chang,J.Y. (2019) New insights into mechanisms of cisplatin resistance: from tumor cell to microenvironment. *Int. J. Mol. Sci.*, **20**, 4136.
65. Bouwman,P. and Jonkers,J. (2012) The effects of deregulated DNA damage signalling on cancer chemotherapy response and resistance. *Nat. Rev. Cancer*, **12**, 587–598.
66. Rocha,C.R.R., Silva,M.M., Quinet,A., Cabral-Neto,J.B. and Menck,C.F.M. (2018) DNA repair pathways and cisplatin resistance: an intimate relationship. *Clinics (Sao Paulo)*, **73**, e478s.
67. Chen,Q., Cai,D., Li,M. and Wu,X. (2017) The homologous recombination protein RAD51 is a promising therapeutic target for cervical carcinoma. *Oncol. Rep.*, **38**, 767–774.
68. Hengel,S.R., Spies,M.A. and Spies,M. (2017) Small-molecule inhibitors targeting DNA repair and DNA repair deficiency in research and cancer therapy. *Cell Chem. Biol.*, **24**, 1101–1119.
69. Volcic,M., Karl,S., Baumann,B., Salles,D., Daniel,P., Fulda,S. and Wiesmuller,L. (2012) NF-kappaB regulates DNA double-strand

break repair in conjunction with BRCA1-CtIP complexes. *Nucleic Acids Res.*, **40**, 181–195.
70. Lim,G., Chang,Y. and Huh,W.K. (2020) Phosphoregulation of Rad51/Rad52 by CDK1 functions as a molecular switch for cell cycle-specific activation of homologous recombination. *Sci. Adv*,. **6**, eaay2669.
71. Prado,F. (2018) Homologous recombination: to fork and beyond. *Genes (Basel)*, **9**, 603.
72. Huang,R.X. and Zhou,P.K. (2020) DNA damage response signaling pathways and targets for radiotherapy sensitization in cancer. *Signal Transduct. Target Ther.*, **5**, 60.